UNIVERSITY OF CALIFORNIA, SAN DIEGO

The Use of Optical Tweezers and Laser Scissors in Cell Biology: Sperm Motility and Nerve Regeneration

A Thesis submitted in partial satisfaction of the requirements for the degree Master of Science

in

Bioengineering

by

Nicholas W. Hyun

Committee in charge:

Professor Michael Berns, Chair
Professor Peter Yingxiao Wang
Professor Michael Heller

2014

The Thesis of Nicholas W. Hyun is approved, and it is acceptable in quality and form for publication on microfilm and electronically:

_____

_____

_____

Chair

University of California San Diego

2014

Dedication

To my parents, Kim, and Hephzibah for supporting me throughout my life and education. I would also like to thank Michelle for her love and support.

Table of Contents

List of Figures

List of Tables

Acknowledgements

I am very grateful to have worked with some remarkable individuals during my undergraduate and graduate school career. These individuals have had a profound impact on my personal and scientific development.

I would like to thank Professor Michael Berns for being an extraordinary mentor and advisor. His support and confidence in me has allowed me to grow as researcher. I could not have gotten to where I am now without his vast knowledge and experience.

I would like to thank Dr. Linda Shi for seeing my potential as an undergraduate. She always looked out for me and kept me on track. I am very thankful for her help and expertise in optics and programing.

I would like to thank Charlie for mentoring me throughout my undergraduate and graduate career. Charlie was always willing to help me with any question I had. I was always impressed by his knowledge and his ability to simplify concepts to teach me.

I would like to thank Michelle for helping me with my cell cultures and offering excellent advise on my research.

I would like to thank Veronica for helping me with my cell cultures and teaching me immunofluorescence staining. I also would like to thank Veronica for her cheerful attitude and willingness to help me with any question I had. I always enjoyed our conversations on science and life.

I would like to thank Qingyuan for his knowledge on optics and for helping me with RBLI.

I would like to thank Daryl for his knowledge on optics and image processing. From our brief time working together, I am confident he will make a wonderful addition to our lab both in his knowledge and personality.

I would like to thank Aaron, Sean, Colin, Kyle, and Selin for their hard work and helping me with my research.

I would like to thank Chia-Chun, April, and Orlangie from the Mobley lab for help me with my cell cultures. My research would not have been possible without their help.

I would also like to thank Sol from the Goldstein lab for providing me IPS nerve cells.

Finally I would like to thank my other colleagues and friends from the UCSD over the years including Chris Lee, Sandro Jaeggi, Sean Luong, Chris Hara, Nick Kunzer, Gus Patton, Marco Maruggi, David Oda, Stuart Ipsen, Carolyn Schutt-Ipsen and many others. From late night study sessions to early morning surf sessions, I want to thank everyone for helping get through my education.

The material presented in Chapter 1 is, in full, a reprint of the material as it appears in "Effects of Viscosity on Sperm Motility Studied with Optical Tweezers," by Nicholas Hyun, Charlie Chandsawangbuwana, Qingyuan Zhu, Linda Z. Shi, Collin Yang-Wong, and Michael W. Berns. Journal of Biomedical Optics 17(2), 2012. The thesis author primary investigator and first co-author of this paper.

Chapter 2, in part, is a reprint of material as it appears in " Laser Microbeam Targeting of Single Nerve Axons in Cell Culture" Methods in Molecular Biology: Neuronal Cell Death, 2014, Nicholas Hyun, Linda Z. Shi, and Michael W. Berns. The thesis author was the primary investigator and author of this material.

ABSTRACT OF THE THESIS

The Use of Optical Tweezers and Laser Scissors in Cell Biology: Sperm Motility and Nerve Regeneration

by

Nicholas W. Hyun

Master of Science in Bioengineering

University of California, San Diego, 2014

Professor Michael Berns, Chair

Optical tweezers and laser scissors are invaluable tools to manipulate cells on the micro and nano scale level. By integrating laser technologies with imaging and biochemical techniques, robust systems can be created to study various biological and biochemical processes. The purpose of this thesis is to describe two different optical methods used to study two cell-based problems. In the first experiment, optical

tweezers are used to examine the effects of viscosity on sperm motility and energetics using a 1064nm Nd:YVO_4 continuous laser. In the second experiment, laser scissors are used to study growth cone response from laser induced damage using a Vanguard Nd: YVO_4 second harmonic generator (SHG) 532 nm picosecond green laser. The proceeding sections describe the optical systems for each experiment as well as the methods used. Results of both studies are presented and discussed in detail.

Introduction

Optical trapping

There are many methods to describe the forces involved in optical traps. Ray optics is a particular successful model for optical properties on particles much larger than the wavelength of light because wave effects can be averaged [1]. Photons of light possess a momentum that can be imparted to an object. As light rays pass through an object, the ray optics of the light changes in its direction, intensity, and polarization due to the refractive index of the object [2]. The change in ray direction results in a change of momentum that is imparted on the object. Optical traps advantageously use this principle and the conservation of momentum to create forces to confine and manipulate microscopic objects.

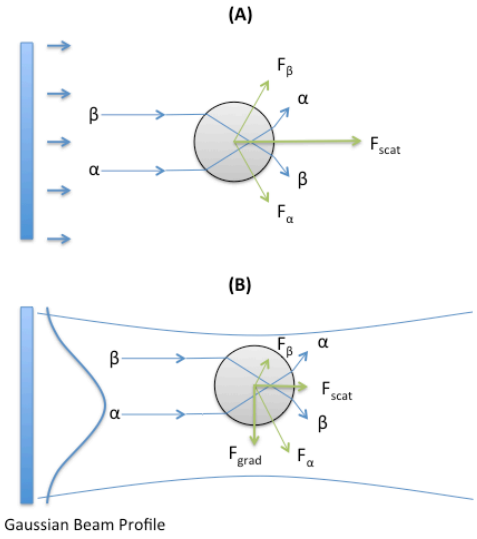

Figure 1: Ray Optics description of an optical trap.

The interaction of light rays and a spherical particle can be summarized in Figure 1. As ray "α" hits the spherical particle, it is refracted as shown in Figure 1a. Apart from minor surface reflection that we neglect, it emerges from the sphere at the same angle as it entered [3]. The refraction creates a force F_α in the direction of the momentum change due to the conservation of momentum. Similarly ray "β" creates force F_β that is symmetrical to F_α. Adding the vector components of F_α and F_β and other similar rays, a net force is created on the sphere in the direction of the incident light called the scattering force [3]. In Figure 1B, the same principles of ray optics are applied to a Gaussian beam. Force F_α will be larger than F_β due to the intensity gradient of the Gaussian beam. When adding the vector components of the incident rays, a net inward force is created transversely to the incident of light. This is called the gradient force. The scattering force acting in the direction of the light and the gradient force drawing the particle to the new focus point are created by the light refraction [3]. For the optical trap to be stable, the gradient force must be greater than the scattering force. To achieve sufficient gradient forces, a laser is focused to a diffraction limited spot using high numerical aperture objectives. Additionally the refractive index of the particle needs to be greater than the refractive index of the surround media. The magnitude of force an optical trap can exert on an object is described by equation:

$$f = \frac{nP}{c} \times Q$$

where n is the index of refraction of the surround media, P is the laser power, c is the speed of light, and Q is the dimensionless force efficiency (the % of the momentum

transferred to the object). This value is the force efficiency of the trap and can also be view as the fractional momentum change per photon [1].

The ability to confine and apply force to microscope objects makes optical traps useful tools in biology for studying cell structures and functions. A focused 1 um beam using 25-300 mW, can create piconewton forces to move cell organelles and whole cells [4]. When using optical traps in biology, it is important to consider the geometry, size, and angle the incident beam strikes the target. The curved geometry of the target is particular important since it effects how the rays are refracted at the surface, thus the direction and net force created [4]. It is also important to consider the wavelength used to minimize the photothermal and different photochemical effects that may damage the target.

In this thesis, an optical trapping system is used to study the effects of viscosity on sperm motility. By determining the minimum power need to hold a motile sperm in a trap [5], the swimming force of a sperm can be determined by using the force efficiency equation. The sperm head for human cells is around 5um and approximately spherically shaped making it ideal for trapping. Sperm trapping using a 1064 nm laser was shown to have minimal adverse effects on sperm motility due to the low absorption at this wavelength when trapped at 420mW for less than 10 seconds [5].

Laser scissors

As laser technologies improved researchers began exploring the potential of using lasers in biology and medicine [6]. Early studies by Berns et al. showed that highly focused lasers could be used as a tool to cut and make incisions within a cell [7, 8, 9]. The use of laser microbeams to modify cells and intracellular structures became known as "laser microsurgery". The advancement of microsurgery proceeded with the development of the solid-state q-switched neodynmium:yttrium aluminum garnet (Nd:YAG) laser which allowed for wavelengths to be harmonically generated at 532 nm (green) 355nm (UV), and 266nm (UV) [4]. Nd:YAG lasers could produced beams with pulses in the nanosecond and picosecond ranges with hundreds of millijoules per pulse. This technology allowed precise subcellular damage using mostly nonlinear absorption, instead of previous linear absorption of biological chromophores. The possibility of multi-photon effects of a focused laser into a live cell through a microscope was suggested by Berns in 1976, and described and demonstrated by Calmettes and Berns in 1983 [6, 10]. Recently such technologies have been shown to be applicable to damaging nerve axons in culture to observe damage-repair and growth cone sensing, using a 532 nm nanosecond pulsed laser [11].

To achieve the spatial resolution required for microsurgery, a pulsed laser is focused to a diffraction limited spot. Gaussian mode (TEM_{00}) of beams are essential because their properties allow the laser beam to be focused to the diffraction limit to create the minimum spot size achievable by an optical system [12]. The radius of the diffraction-limited spot is a function of the numerical aperture of the objective where higher numerical apertures allow the beam to be focus to smaller spot sizes. When

performing laser microsurgery, the damage created with short pulsed lasers is dependent on the irradiation of the laser beam and the pulse duration i.e. nano, pico, fento second pulses.

In this study, laser microsurgery is performed using a Nd: YVO_4 532 nm picosecond pulsed laser instead of 532 nm nanosecond pulsed laser used previously to damage nerve axons. The subcellular damage created using the picosecond laser vs. the nanosecond laser are in principle the same [13]. The damage created most likely involves multiphoton absorption or optical breakdown due to the generation of a microplasma with high electric fields and consequent acousto-mechanical effects [4]. The difference in pulse duration affects the non-linear properties of the laser. In the picosecond regime, multiphoton ionization is more prevalent in the optical breakdown process because there is less time available for the avalanche ionization process. As a result, the threshold for optical break down is significantly higher than in the nanosecond range creating microplasmas smaller in volumetric energy than a nanosecond pulse. This lowers the severity of direct vaporization and damage caused by the cavitation bubbles [6]. These characteristics of the picosecond laser make it ideal for creating laser scissors with better precision and wider range of useable picosecond pulses [6].

References

1. H. Rubinsztein-Dunlop, A. B. Stilgoe, D. Preece, A. Bui, and T. A. Nieminen. (2013). Optical Forces, trapping and Manipulation. In D. Andrew (ed.), *Photonics* (1st ed.). Hoboken, New Jersey Chapter: Jowhn Wiley & Sons, Inc.

2. A. Ashkin. (1992). Forces of a single-beam gradient laser trap on a dielectric sphere in the ray optics regime. *Biophys. J.* **61**, 569-582.

3. A. Ashkin. (1997). Optical trapping and manipulation of neutral particles using laser. *PNAS.* 94 (10), 4853-4860.

4. M.W. Berns, Y. Tadir, H. Yiang, and B. Tromberg (1998). Laser Scissors and Tweezers. *Methods in Cell Biology* (Vol 55). Academic Press

5. J. M. Nascimento, E. L. Botvinick, L. Z. Shi, B. Durrant and M. W. Berns, Analysis of sperm motility using optical tweezers, *Journal of Biomedical Optics*, **11**(044001 (2006).

6. P.A. Quinto-Su, and V. Venugopalan. (2007) Mechanism of Laser Cellular Microsurgery. In M.W. Berns and K.O. Greulich (ed.) *Methods in Cell Biology*. Vol. 82. London, Uk Elsevier

7. M.W. Berns, R.S. Olson, and D.E. Rounds (1969). In vitro production of chromosomal lesions using an argon laser microbeam. *Nature* 221(5175, 74-75)

8. M.W. Berns, W.K. Cheng, A.D. Floyd, and Y. Ohnuki (1971). Chromosomes lesions produced with argon laser microbeam without dye sensitization. Science 171(3974, 903-905).

9. M.W. Berns, J. Aist, J.Edwards, K. Strahs, J. Girton, P. McNeill, J.B. Rattner, M. Kitzes, M. Hammer-Wilson, L.H. Liaw, A. Siemens, M. Koonce, S. Peterson, S. Brenner, J. Burt, R. Walter, P.J. Bryant, D. van Dyk, J. Coulombe, T. Cahill, G.S. Berns. (1981). Laser microsurgery in cell and developmental biology. Science 213(4507), 505-513

10. Berns, M. W. A possible two-photon effect in vitro using a focused laser beam. Biophys. J. 16: 973-977, 1976.

11. T. Wu, S. Mohanty, V. Gomez-Godinez, L.Z. Shi, L.H Liaw, J. Miotke, R.L. Meyer, and M.W. Berns. (2011) Neuronal growth cones respond to laser-induced axonal damage. *J R Soc. Interface*

12. W.T. Silfvast (1996). Laser Fundamentals. Cambridge, New York, NY

13. A. Vogel, and V. Venugopalan. (2003) Mechanisms of pulsed laser ablations of biological tissues. Chem. Rev. 103(2), 577-644.

Chapter 1

Optical Tweezers:

Effect of Viscosity on Sperm Motility

Abstract

The purpose of this study is to analyze human sperm motility and energetics in media with different viscosities. Multiple experiments were performed to collect motility parameters using a customized computer tracking software that measures the curvilinear velocity (VCL) and the minimum laser power (Pesc) necessary to hold an individual sperm in an optical trap. The Pesc was measured by using a 1064nm Nd:YVO_4 continuous wave laser that initially optically traps motile sperm at a power of 450mW in the focused trap spot and subsequently reduces the laser power until the sperm is able to swim out. The VCL was measured frame by frame before trapping. In order to study sperm energetics under different viscous conditions, sperm were labeled with the fluorescent dye $DiOC_6$ to measure membrane potentials of mitochondria in the sperm midpiece. Fluorescence intensity was measured before and during trapping. The results demonstrated a decrease in VCL but and increase in Pesc with increasing viscosity. Fluorescent intensity is the same regardless of the viscosity level indicating no change in sperm energetics. The results suggest that, under the conditions tested, viscosity physically affects the mechanic properties of sperm motility rather than the chemical pathways associated with energetics.

Introduction

Sperm motility, the ability of a sperm to move efficiently towards the egg, is a valuable parameter in the assessment of sperm quality and fertilization capacity [1].

The ability to evaluate sperm motility is important in areas such as sperm cryopreservation, in-vitro fertilization (IVF), and artificial insemination (AI). Factors in the vaginal canal, such as pH, antibody response, and the overall structural and functional capacity of the sperm, can affect sperm motility [2]. Particularly, the viscous environment encountered by the sperm can have a major impact on its motility and its subsequent ability to reach and fertilize the egg. The objective of this study is to address the relationship between viscosity and sperm motility using optical trapping.

There are various methods to score and quantify sperm motility. Computer aided analysis quantifies the overall motility of a sperm population in a short amount of time [3, 4]. Commercial computer assisted sperm analysis (CASA) systems have been developed to track sperm within a field of view and measure motility parameters such as curvilinear velocity (VCL), amplitude of lateral head movement, and percent of motile sperm [3, 4]. Examples of these commercial systems include Hamilton Thorne IVSO- CASA, SM-CMA (Stromberg-Mika, Bad Feilnbach, Germany), and the Hobson Sperm Tracker (Hobson Sperm Tracking LTD, Sheffield, UK). Other optically based computer aided tacking systems such as the real-time automated tracking and trapping system (RATTS) have been developed to automatically tack and optically trap individual sperm [5]. RATTS can measure VCL and has the added ability to measure sperm swimming force using optical tweezers to hold and release individual sperm [6]. Optical tweezers (traps) can confine and manipulate microscopic particles due to the momentum of photons in a tightly focused laser beam [7, 8]. RATTS utilizes optical tweezers to quantify sperm swimming forces by measuring the

minimum amount of laser power need to hold the sperm in the trap. The laser escape power (Pesc) is directly proportional to the sperm's swimming force and can be calculated using the equation, F=QP/c, where F is the swimming force, P is the laser power, c is the speed of light in the medium, and Q is the geometrically determined trapping efficiency parameter [9]. Previous studies have used optical tweezers to noninvasively study sperm motility by measuring swimming forces [6, 9]. The development of RATTS permits simultaneous measurement of force and VCL thus providing a multiparametric analysis of sperm motility.

The goal of this study is to analyze the effect of viscosity on sperm motility by measuring both VCL and sperm swimming force using RATTS. A membrane potential-sensitive fluorescent probe is also used to examine changes in the sperm energetics as a function of changes in viscosity of the swimming medium. Fluorescent probes have been used to relate mitochondrial membrane potential to sperm motility and have demonstrated that high mitochondrial membrane potentials in the sperm midpiece correlate with an increase in ATP synthesis and increased motility [10]. Cyanine dyes such as 3,3'-dihexyloxacabocyanine iodide $DiOC_6$ (3) integrate into the mitochondria and increase in fluorescence intensity as the magnitude of the membrane potential increases. There are numerous chemical probes to measure mitochondrial activity, such as carbocyanines $DiOC_2$ (6), $DiOC_6$ (3), rhodamine (TMRE, JC-1), and rosamine (CMX-ROS). $DiOC_6$ (3) is used in this study because it has been demonstrated to be an effective dye for measuring membrane potentials in sperm [11].

Methods and Materials

Optical System

The optical system is described in Figure 1.1. Briefly, it uses a Nd: YVO_4 continuous wave 1064 nm wavelength laser (Spectra Physics, BL-106C, Mountain View, CA) which travels though as series of lenses and mirrors into a Zeiss Axiovert S100 microscope and a 40x, Phase II, NA 1.3 oil immersion objective (Zeiss, Thornwood, NY) where it is focused to a diffraction-limited spot of approximately 1 um^2. A motorized rotating ½ wave plate controls the laser power by attenuating the laser beam during the sperm swimming force experiments. The beam-expanding lenses and focusing lens fill the objective back aperture with collimated laser beam maximizing the amount of energy in the trapping focal spot.

The optical system for acquiring phase and fluorescence images have been describe previously [11]. Briefly, a Zeiss fluor arc lamp provides the excitation light. A red filter above the image plane allows for the separation of phase contrast (670 nm) and fluorescence (500 to 570 nm) images. The reflected phase contrast is collected by a charged coupled device (CCD) camera (Cohu model 7800, San Diego, CA) at 40 fps. The fluorescence information passes through a HQ 500/20nm emission filter and is collected by a digital camera (Quantix 57, Roper Scientific Inc. Tuscon, AZ).

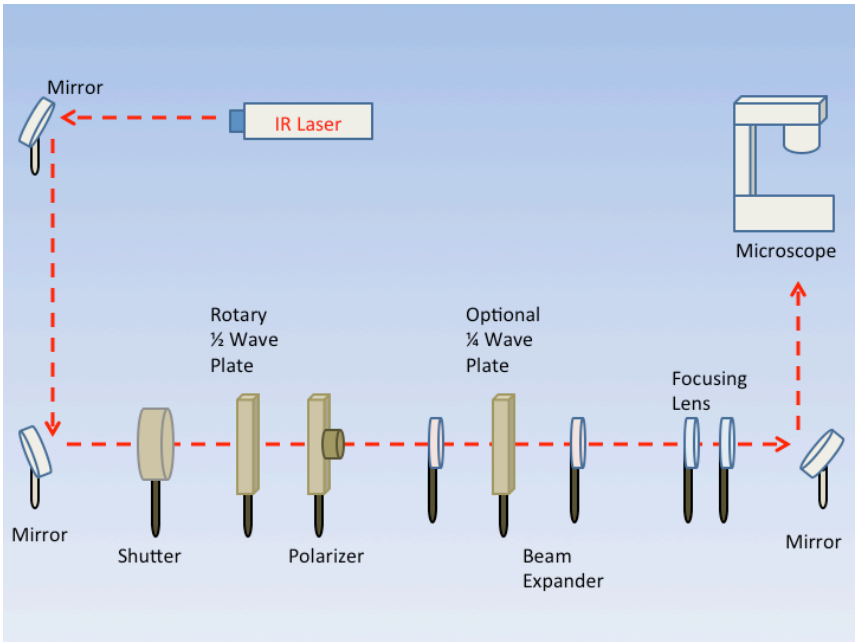

Figure 1.1: Optical trapping system used for sperm motility studies.

Hardware and Software System

Motility parameters were measured using two computer-based analysis systesm. First, CASA (IVOS Sperm Anlyzer, Hamilton Thorne, Bervely, MA) was used to assess the initial quality of sperm samples and to measure VCL. Second, VCL and Pesc were measured simultaneously using a customized software tracking and trapping software (RATTS) coded in the LabView language (National Instruments, Austin, TX). RATTS operates at a 40 fps video rate and provides remote robotic interfaces with the hardware. In addition, the system has fluorescent image processing capabilities [5]. The operation of RATTS is performed in the upper-level system while the fluorescent image acquisition, processing, and storage are done in the lower-level system, as shown in Figure 1.2. The two computers are networked together over a

gigbit TCP/IP cat5e crossover connection. Communication between the two systems is optimized with LabView's Shared variables and virtual instrument (VI server function in which the lower-level system continuously polls the upper-level system for the next request. Using RATTS, sperm are tracked for an extended duration before and after laser trap experiments. Motility measurements including VCL are measured followed by subsequent trapping measurements. A more detailed description of the system has been presented previously [13].

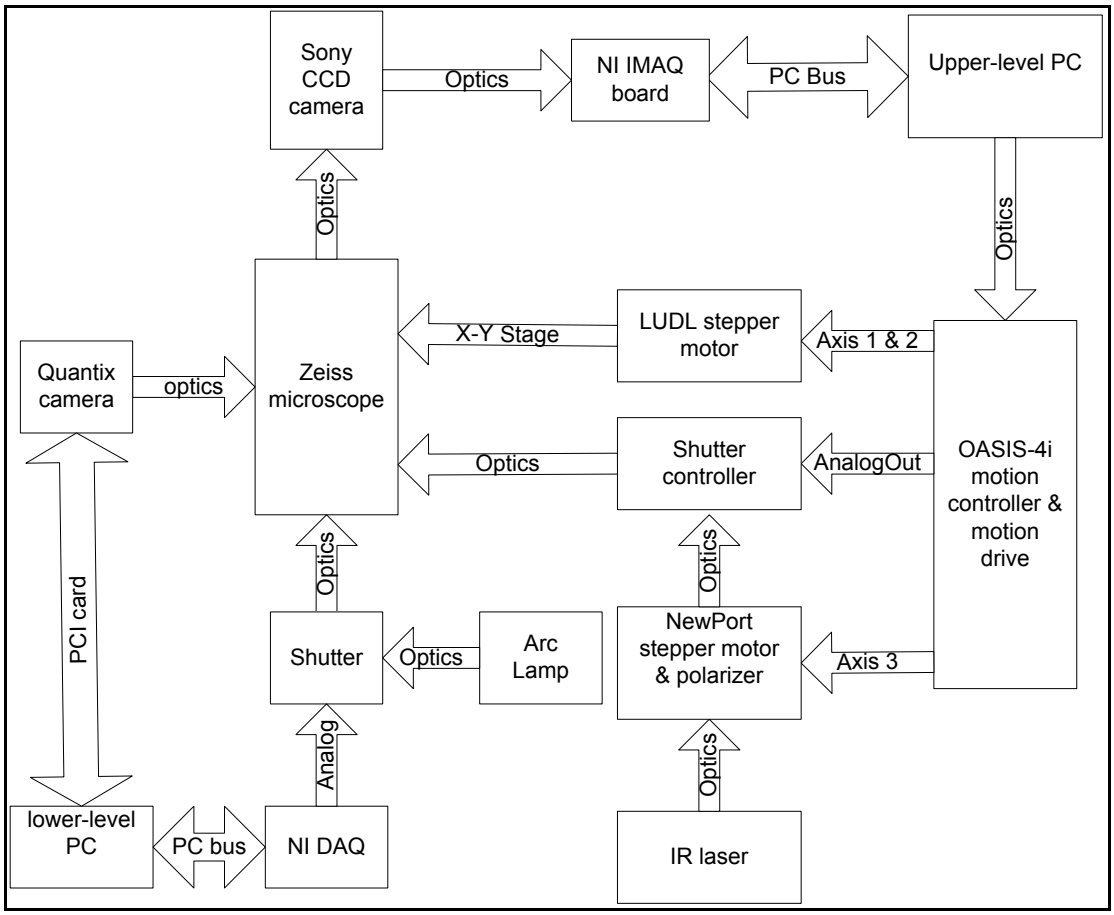

Figure 1.2: Hardware diagram of system to study sperm motility and energetics. Abbreviations: charge-coupled device (CCD); data acquisition (DAQ); image acquisition (IMAQ); infrared (IR); personal computer (PC); peripheral component interconnect (PCI), National Instruments (NI)

Sperm Collection and Preparation with $DiOC_6$

Human samples were supplied by Infertility, Gynecology, and Obstetrics Medical Group (La Jolla, CA). The samples were frozen according to a normal human freezing protocol [14, 15, 16]. Human sperm samples were thawed in a water bath at 37° C for 2 min, and then centrifuged for 10 min at 2000 rpm. The supernatant was removed and the pellet was re-suspended in 1mL of HEPES buffered modified Human Tubal Fluid (mHTF) with filtered 5% serum substitute supplement (SSS) (Irvine Scientific, Irvine, CA). The sample was again centrifuged for 10 min at 2000 rpm and resuspended. This two-wash technique was used for all experiments. The final sperm dilutions of 30,000 sperm per mL were loaded into cover slide dishes (about .5 uL of sperm in 2.5 mL methylcellulose+mHTF+SSS media) and mounted on the microscope stage [11].

For fluorescent studies 3,3'-dihexyloxacarbocyanine iodide ($DiOC_6(3)$, Invitrogen, Carlsbad, CA), a non-ratiometric, carbocyanine dye, was added to the prepared sperm; 40 nM stock $DiOC_6(3)$ dye was added into 250 μL of prepared human sperm and was incubated at 37° C for 20 min [11]. The sperm sample was loaded into the optical system to measure midpiece mitochondrial fluorescence. Stock solutions of $DiOC_6(3)$ dye were prepared with dimethyl sulfoxide (DMSO).

Viscous Media Preparation

Media with different viscosities were created by varying the concentration of methylcellulose (Sigma Aldrich M 7140, St. Louis, MO) in mHTF+5%SSS sperm

suspension media. Specifically, media with viscosities of 3 cP, 6 cP, 9 cP, and 15 cP were made by adding .5%, 1%, 1.5%, and 2% (w/w) methylcellulose (Sigma Aldrich M 7140) to the media respectively. Initially 1/3 of the mHTF was heated to 80° C. The methylcellulose powder was added to the heated mHTF media, and the mixture was agitated until the particles were evenly dispersed. For complete solubilization another 1/3 of the mHTF media was added as cold media to lower the temperature of dispersion. The final 1/3 of the mHTF media was added along with SSS to yield a final mHTF+5% SSS solution with the desired methylcellulose concentration. The solution was agitated and subsequently cooled to 0 – 5° C for 20 – 40 minutes to lower the temperature of dispersion and further hydrate the methylcellulose. The solution was then continuously agitated for an additional 30 minutes after the proper temperature was reached.

Refractive Index Analysis

The refractive indices of the viscosity solutions were measured using a digital refractometer (Sper Scientific model 300034, Scottsdale, AZ) with an instrument range of 1.330 – 1.5318, resolution of 0.0001, and accuracy of ±0.0002. Measurements were taken at 22.3° C using 1 mL of solution. The refractive index of a sperm cell was approximated to be 1.53 [17]. The effects of refractive index on optical trap stiffness was considered by comparing the difference between the sperm cell refractive index and the media refractive indices [18].

Statistical Analysis

Comparisons between experimental data sets were performed in MATLAB (Mathworks, Natick, MA) using the nonparametric Wilcoxon rank sum test (based on 5% significance). The experimental results are presented in Figures 1.3–1.6 as box plots. Each box plot displays the following data: median (center line of box), upper and lower quartile values (top and bottom of box, respectively), range (upper and lower bars), and data points lying outside 3-times the interquartile range. The notches of the box plots represent the uncertainly of the median value. If the notches do not overlap, then the medians are different at the 95% confidence level

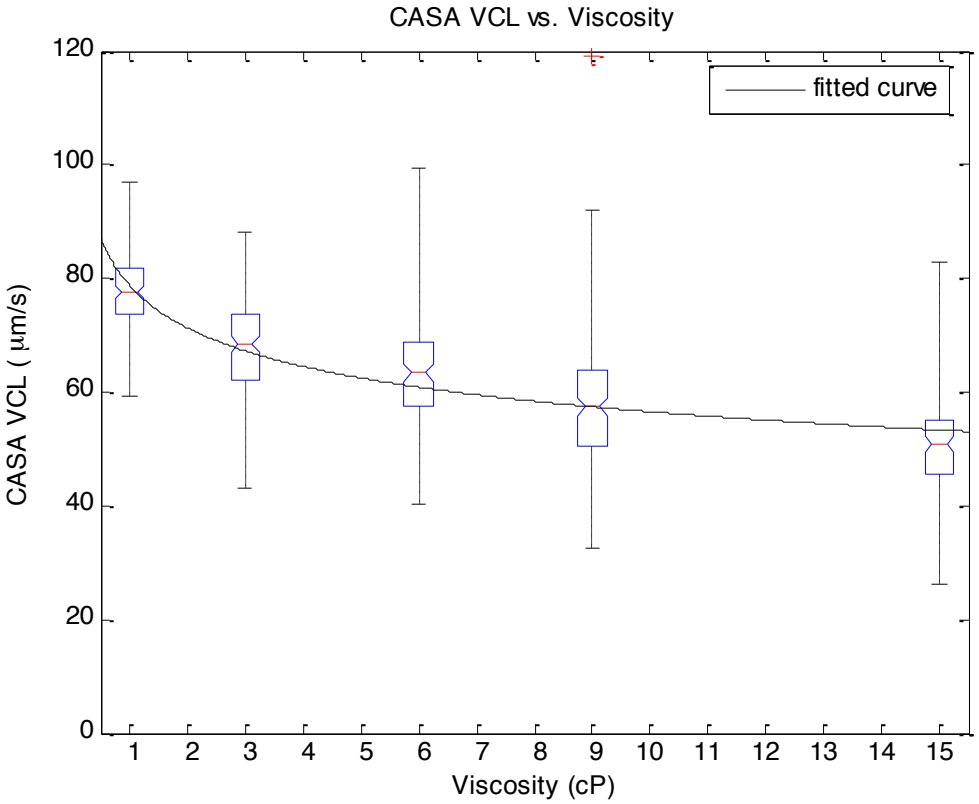

Figure 1.3: CASA VCL vs. Viscosity. MATLAB was used to fit a power model (y = a*xb) to the medians of the data sets. The coefficients with their 95% confidence limits were found to be a = 78.83 (72.3, 85.35) and b = -0.1442 (-0.1952, -0.9315) yielding the equation y = 78.83*(x-0.1442). The correlation coefficient was determined to be R2 = 0.9656. N-values at 1 cP (n=1452), 3 cP (n=1744), 6 cP (n=1295), 9 cP (n=1715), and 15 cP (n=1471).

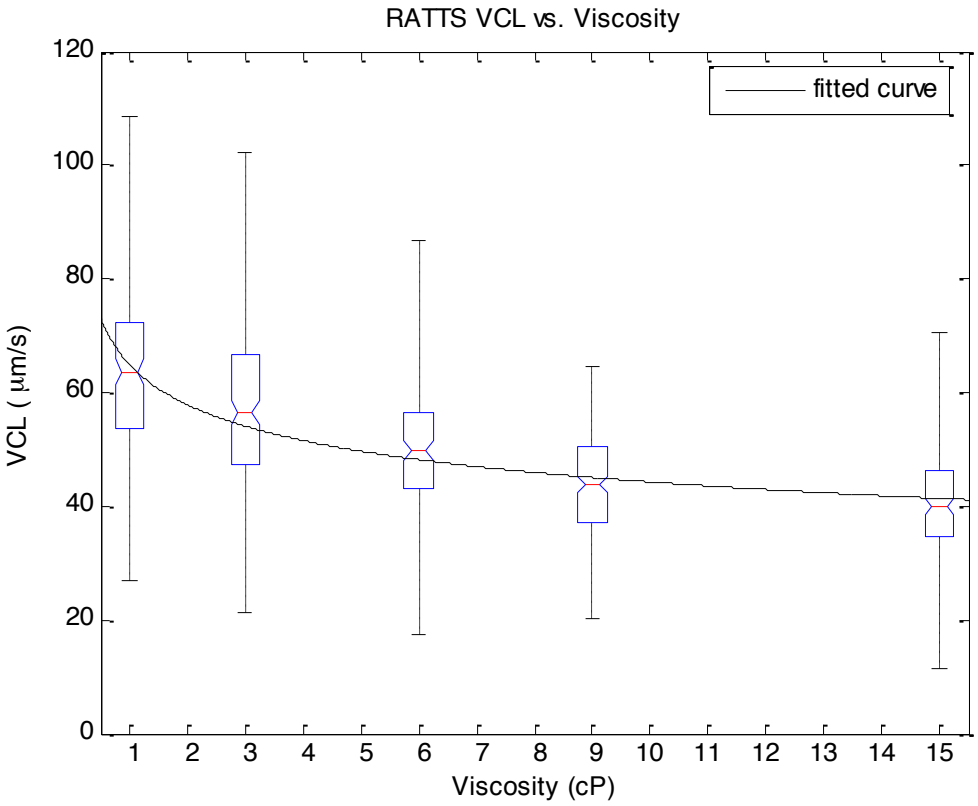

Figure 1.4: RATTS VCL vs. Viscosity. MATLAB was used to fit a power model (y = a*xb) to the medians of the data sets. The coefficients with their 95% confidence limits were found to be a = 64.99 (58.88, 71.1) and b = -0.1668 (-0.226, -0.1076) yielding the equation y = 64.99*(x-0.1668). The correlation coefficient was determined to be R2 = 0.9513. N-values at 1 cP (n=173), 3 cP (n=188), 6 cP (n=207), 9 cP (n=217), and 15 cP (n=188).

Results

For each sperm sample, motility parameters were first analyzed at 1 cP (mHTF media with 5% SSS and no methylcellulose) using the CASA system where the VCL could be closely monitored in multiple fields of view. This measurement served as an initial base-line for sperm quality/motility before subsequent experiments were preformed. CASA was then used to measure VCL at 3 cP, 6 cP, 9 cP, and 15 cP. The CASA VCL parameters were aggregated and graphed using MATLAB (Figure 1.3).

The CASA VCL results demonstrate a decrease in VCL with increasing viscosity. A power model ($y = a*x^b$) was fitted to the medians of the data sets yielding the equation $y = 78.83*(x^{-0.1442})$ with a correlation coefficient of $R^2 = 0.9656$. The same sperm samples were then measured for VCL using RATTS. The aggregated data was graphed and fitted to a power model yielding the equation $y = 64.99*(x^{-0.1668})$ with a coefficient of $R^2 = 0.9513$. Although the VCL measurements from RATTS were slightly lower than those from CASA, a similar relationship between VCL and viscosity was observed with a confidence level greater than 95% (Figure 1.4).

Pesc measurements were then performed using RATTS in 1 cP, 3 cP, 6 cP, 9 cP, and 15 cP media (Figure 1.5). A power model was fitted to the medians of the data sets yielding $y = 2.953*(x^{1.824})$ with a correlation coefficient of $R^2 = 0.9775$. The results reveal that at higher viscosities the sperm escape from the laser trap at higher laser powers. This indicates that the sperm swim with greater force as viscosity increases. Statistical analysis of the data sets reveal that the Pesc at 1cP:6cP, 1cP: 9cP, and 1cP:15cP are statistically different ($p < .05$) with p-values of $p = 3.11E-04$, $p = 1.35E-08$, and $p = 2.51E-11$ respectively. However at 1cP:3cP, the Pesc was found to be statistically the same ($p > 0.5$) with a p-value of 0.6887. The statistical analysis indicates that viscosity affects sperm swimming force in viscosities higher than 3cP.

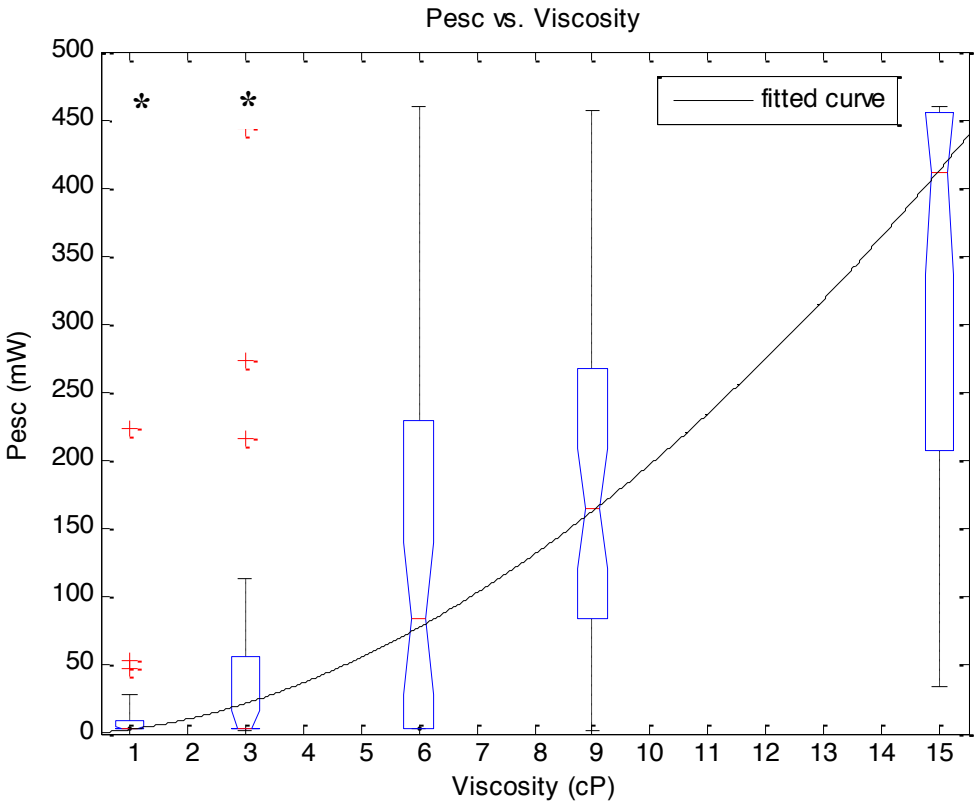

Figure 1.5: Pesc vs. Viscosity. MATLAB was used to fit a power model (y = a*xb) to the medians of the data sets. The coefficients with their 95% confidence limits were found to be a = 2.953 (0.334, 5.573) and b = 1.824 (1.486, 2.163) yielding the equation y = 2.953*(x1.824). The correlation coefficient was determined to be R2 = 0.9775. N-values at 1 cP (n=35), 3 cP (n=39), 6 cP (n=41), 9 cP (n=44), and 15 cP (n=27). The asterisks (*) indicate that there was no significant difference between 1 cP and 3 cP at 5% confidence level.

To examine if aerobic energetics plays a role in this phenomenon, sperm were incubated in media containing the membrane potential-sensitive dye $DiOC_6(3)$ following the protocol previously described [11]. The $DiOC_6$ treated sperm were tested in viscosities of 1cP, 6cP and 9cP. The fluorescence data were aggregated and graphed (Figure 1.6). The data sets of 1cP:6cP and 1cP:9cP were statistically compared using the Wilcox Rank Sum test, and yielded p = 0.6023 and p =0.8874 respectively. These results indicate that there is no significant change with a

confidence of $p > 0.5$. Therefore, it does not appear that there is an increase in mitochondrial ATP generation as the sperm encounter higher viscosities even though they are escaping from the trap with greater force.

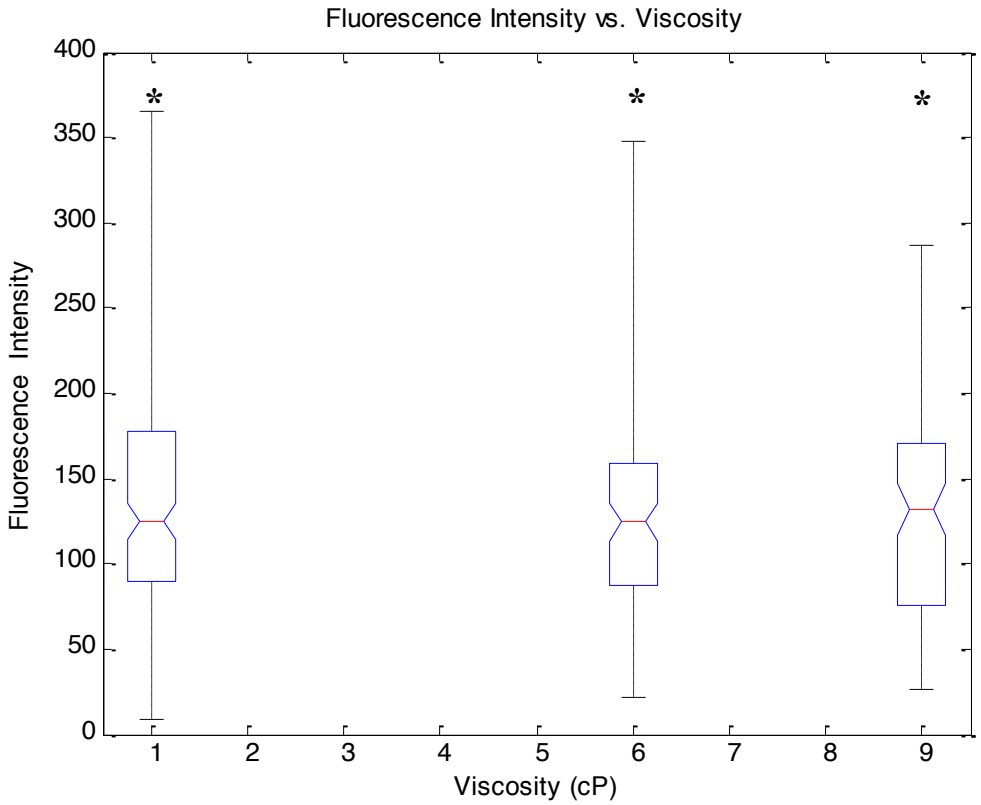

Figure 1.6: Fluorescence vs. Viscosity. Midpiece fluorescence intensity of DiOC6(3) treated sperm was measured. Asterisks (*) indicates that there was no significant difference in fluorescence intensity between 1 cP:6 cP and 1 cP:9 cP at the 5% level. N-values at 1 cp (n=172), 6 cP (n=98), and 9 cP (n=95). Fluorescence intensity was measured by subtracting the background intensity (sperm samples without fluorescence probe) from the fluorescence measurements using DiOC6(3).

The refractive indices of the solutions were measured using a digital refractometer with a resolution of 0.0001 and an accuracy of ±0.0002 (Table 1). The index of refraction ranged from 1.3361±0.0002 at 1 cP to 1.3387±0.0002 at 15 cP. As

the concentration increased, the index of refraction proportionally increased at a rate of approximately 0.0013 per 1% methylcellulose.

Table 1.1: Refractive indices of the viscosity solutions

Solution	Viscosity (cP)	Refractive Index
mHTF + 5% SSS	1	1.3361
mHTF + 5% SSS + 0.5% methylcellulose	3	1.3368
mHTF + 5% SSS + 1.0% methylcellulose	6	1.3374
mHTF + 5% SSS + 1.5% methylcellulose	9	1.3381
mHTF + 5% SSS + 2.0% methylcellulose	15	1.3387

Discussion

VCL measured on both the CASA and RATTS systems show that as the viscosity increases, VCL decreases. This result is not surprising considering basic principles of fluid mechanics: an object moving through a fluid is subjugated to frictional forces created by the viscosity of the medium. Increasing the viscosity of the mHTF medium augments the fluid's ability to resist shear stress. Thus as viscosity increases, sperm velocity should decrease. Although sperm swim-trajectory is complicated because of its three dimensional waveform, its speed is correlated to

viscosity as fluid flow laws dictate for a linear, non-random traveling object [19]. This trend is modeled using MATLAB to fit the power regression $y = a*(x^b)$ (Figures 1.3 and 1.4). The equation relates viscosity to motility parameters as follows: VCL = $78.83*(\text{Viscosity}^{-0.1442})$ and RATTS VCL = $64.99*(\text{Viscosity}^{-0.1668})$. The power parameter (b) represents the rate at which VCL is decreasing with increasing viscosity. Although the VCL measurements are slightly different, the (b) parameters -0.1442 and -0.1668 fall within the 95% parameter confidence limits for CASA and RATTS respectively (Figure 1.3 and 1.4), and validate the accuracy of each system. A possible explanation for the slight difference in VCL measurements may be due the temperature of the sample; CASA heats the sperm sample to 37° C which can affect viscosity of the solution, and RATTS measurements are made at room temperature 20° C. The viscosity media made for this study were calibrated at room temperature, thus viscosity may have decreased due to the increased temperature, accounting for the increase in sperm VCL.

The Pesc motility parameter (sperm swimming force) measured using the optical tweezers and RATTS, responded differently to increasing viscosity. Interestingly, as the viscosity increases above 3 cP, the Pesc increases. Thus, at higher viscosities the swimming force of the sperm increases. To model this behavior MATLAB was used to fit a power regression producing the equation, Pesc = $2.953*(\text{Viscosity}^{1.824})$. By comparing the VCL and Pesc (b) parameters, it is concluded that viscosity has a significant effect on the swimming force of the sperm. The effect of the methylcellulose on the refractive index and trap stiffness was considered [18]. It was determined that from 1 cP to 15 cP, the index of refraction

increased by 0.0026. This small increase in refractive index was calculated to contribute to a less than 1.5% change in trap stiffness from 1 cP to 15 cP. This small change does not explain the large nonlinear increase in laser power needed to trap sperm at increasing viscosities.

A possible explanation for the increase in sperm swimming force was that sperm energetics (ATP generation) increased in response to the higher viscous environment. The sperm, in an effort to maintain its VCL would increase ATP production in the mitochondrial-rich midpiece. To investigate this possibility the mitochondrial membrane potential-sensitive dye DIOC6 (3) was used to monitor the energetics of the sperm while in the trap using the methods reported previously [11, 12]. However, the experimental results (Figure 1.6) did not reveal any difference in mitochondrial midpiece fluorescence when the sperm were swimming in media of different viscosities. Though these data suggest that the increase in swimming force is not related to an increase in mitochondrial ATP generation (aerobic respiration), future experiments should be conducted with other membrane-potential dyes such as JC1 and DiOC2(3) [12, 20]. In addition, the role of ATP from anaerobic respiration (glycolysis) cannot be ruled out as it has been shown to play a significant role in sperm energetics [12]. Notwithstanding, the data presented in this paper demonstrate that as viscosity increases, sperm swim with greater force, but aerobic energetics remains relatively constant. This leads to the speculation that the increase in swimming force may be due the biomechanical properties of the sperm flagellum. Future studies using high-speed imaging will permit detailed analysis of flagellum

waveform, and should help elucidate the biomechanical effect of viscosity on sperm motility [21].

This study has focused on low viscosities, which encompass the 4-10 cP range found in the human male reproductive tract [22, 23, 24]. Future studies examining higher viscosity environments will provide insight into a sperm's journey through human female reproductive tract consisting of viscosities upwards of 1700 cP [24, 25]. In order to do these experiments, higher power laser traps will be needed, and consequent thermal effects of the trap will have to be mitigated [26].

Acknowledgements

This work was supported by funds from the Beckman Laser Institute Inc. Foundation awarded to MWB. CC would like to acknowledge support from a National Defense Science and Engineering Graduate Fellowship and a NSF Graduate Research Fellowship.

Chapter 1, in full, is a reprint of the material published as it appears in "Effects of Viscosity on Sperm Motility Studied with Optical Tweezers" by Nicholas Hyun, Charlie Chandsawangbhuwana, Qingyuan Zhu, Linda Shi, Collin Yang-Wong, Michael Berns. Journal of Biomedical Optics 17(2), 2012. The thesis author was the primary investigator and first author of this paper.

References

1. D. P. Wolf and P. E. Patton, "Sperm cryopreservation: state of the art," *Journal of Assisted Reproduction and Genetics*, **6**(6), 325-327 (1989).

2. J. Rutllant, M. López Béjar, P. Santolaria, J. Yaniz and F. López Gatius, "Rheological and ultrastructural properties of bovine vaginal fluid obtained at oestrus," *Journal of anatomy*, **201**(1), 53-60 (2002).

3. R. P. Amann and D. F. Katz, "Reflections on CASA after 25 years," *Journal of andrology*, **25**(3), 317 (2004).

4. D. Mortimer, *Practical laboratory andrology*, Oxford University Press, USA (1994).

5. L. Z. Shi, J. M. Nascimento, C. Chandsawangbhuwana, M. W. Berns and E. L. Botvinick, "Real-time automated tracking and trapping system for sperm," *Microscopy research and technique*, **69**(11), 894-902 (2006).

6. E. Araujo Jr, Y. Tadir, P. Patrizio, T. Ord, S. Silber, M. W. Berns and R. H. Asch, "Relative force of human epididymal sperm," *Fertility and sterility*, **62**(3), 585-590 (1994).

7. A. Ashkin, "The study of cells by optical trapping and manipulation of living cells using infrared laser beams," *ASGSB bulletin: publication of the American Society for Gravitational and Space Biology*, **4**(2), 133 (1991).

8. A. Ashkin, "Forces of a single-beam gradient laser trap on a dielectric sphere in the ray optics regime," *Biophysical Journal*, **61**(2), 569-582 (1992).

9. K. Konig, L. Svaasand, Y. Liu, G. Sonek, P. Patrizio, Y. Tadir, M. W. Berns and B. J. Tromberg, "Determination of motility forces of human spermatozoa using an 800 nm optical trap," *Cell Mol Biol (Noisy-le-grand)*, **42**(4), 501-509 (1996).

10. C. Marchetti, N. Jouy, B. Leroy-Martin, A. Defossez, P. Formstecher and P. Marchetti, "Comparison of four fluorochromes for the detection of the inner mitochondrial membrane potential in human spermatozoa and their correlation with sperm motility," *Human Reproduction*, **19**(10), 2267 (2004).

11. T. Chen, L. Z. Shi, Q. Zhu, C. Chandsawangbhuwana and M. W. Berns, "Optical tweezers and non-ratiometric fluorescent-dye-based studies of respiration in sperm mitochondria," *Journal of Optics*, **13**(044010 (2011).

12. J. M. Nascimento, L. Z. Shi, J. Tam, C. Chandsawangbhuwana, B. Durrant, E. L. Botvinick and M. W. Berns, "Comparison of glycolysis and oxidative phosphorylation as energy sources for mammalian sperm motility, using the combination of fluorescence imaging, laser tweezers, and real time automated tracking and trapping," *Journal of cellular physiology*, **217**(3), 745-751 (2008).

13. J. M. Nascimento, E. L. Botvinick, L. Z. Shi, B. Durrant and M. W. Berns, "Analysis of sperm motility using optical tweezers," *Journal of Biomedical Optics*, **11**(044001 (2006).

14. "New guidelines for the use of semen donor insemination: 1986. The American Fertility Society," *Fertil Steril*, **46**(4 Suppl 2), 93S-110S (1986).

15. S. J. DiMarzo, J. Huang, J. F. Kennedy, B. Villanueva, S. A. Hebert and P. E. Young, "Pregnancy rates with fresh versus computer-controlled cryopreserved semen for artificial insemination by donor in a private practice setting," *American journal of obstetrics and gynecology*, **162**(6), 1483 (1990).

16. P. Serafini and R. P. Marrs, "Computerized staged-freezing technique improves sperm survival and preserves penetration of zona-free hamster ova," *Fertility and sterility*, **45**(6), 854 (1986).

17. C. Van Duijn, C. Van Voorst and G. Hellinga, "Precision measurements of dimensions, shape and mass density of spermatozoan heads in normal and subfertile human males," *European Journal of Obstetrics & Gynecology*, **2**(2), 37-54 (1972).

18. R. R. Brau, J. M. Ferrer, H. Lee, C. E. Castro, B. K. Tam, P. B. Tarsa, P. Matsudaira, M. C. Boyce, R. D. Kamm and M. J. Lang, "Passive and active microrheology with optical tweezers," *Journal of Optics A: Pure and Applied Optics*, **9**(S), 103-112 (2007).

19. D. M. Woolley, "Motility of spermatozoa at surfaces," *Reproduction*, **126**(2), 259 (2003).

20. A. Mei, E. Botvinick and M. Berns, "Monitoring sperm mitochondrial respiration response in a laser trap using ratiometric fluorescence," p. 59302F (2005).

21. D. J. Smith, E. A. Gaffney, H. Gadêlha, N. Kapur and J. C. Kirkman Brown, "Bend propagation in the flagella of migrating human sperm, and its modulation by viscosity," *Cell Motility and the Cytoskeleton*, **66**(4), 220-236 (2009).

22. C. H. Lee, Y. Wang, S. C. Shin and Y. W. Chien, "Effects of chelating agents on the rheological property of cervical mucus," *Contraception*, **65**(6), 435-440 (2002).

23. M. C. Lin, T. C. Tsai and Y. S. Yang, "Measurement of viscosity of human semen with a rotational viscometer," *Journal of the Formosan Medical Association*, **91**(4), 419 (1992).

24. D. B. Troy, "Remington: The Science and Practice of Pharmacy," Philadelphia College of Pharmacy and Science, New York (2005).

25. P. Y. Tam, D. F. Katz and S. A. Berger, "Non-linear viscoelastic properties of cervical mucus," *Biorheology*, **17**(5-6), 465 (1980).

26. Y. Liu, G. J. Sonek, M. W. Berns and B. J. Tromberg, "Physiological monitoring of optically trapped cells: assessing the effects of confinement by 1064-nm laser tweezers using microfluorometry," *Biophysical Journal*, **71**(4), 2158-2167 (1996).

Chapter 2

Laser Scissors: Growth Cone Response from Laser Induced Damage

Abstract

The purpose of this study was to examine growth cone response from laser induced axonal damage in hippocampus and iPS nerve cells. A Nd: YVO_4 532 picosecond laser was used to damage nerve axons. The short pulsed laser was focused to a diffraction limited to precisely target and injure nerve axons in culture without rupturing the cell membrane (sub-axtomy). Subsequent time series images were taken to analyze growth dynamics and axonal recovery. After laser sub-axtomy axons thinned at the damage site initiating a dynamic cytoskeletal remodeling to restore axonal thickness. The growth cone was observed to play a role in the repair process in both hippocampus and iPS nerve cells. Hippocampus cells transduced with RFP tubulin showed a loss of tubulin damage site followed by tubulin polymerization consistent with phase contrast images after subaxotomy. Immunofluorescence staining confirmed structural tubulin damage and initial phases of cytoskeletal remolding at the damage site. These results indicate that there is a repeatable repair response after laser-induced damage.

Introduction

Neuronal growth cones are specialized motile structures that react to environmental cues to guide nerve growth. The repair and reassembly of the growth cone after injury is crucial in the process of nerve regeneration and it is an important step in driving axonal growth to reconnect with its target. Nerves with incomplete growth cone regeneration often exhibit dystrophic end bulbs which are markers for

degenerating axons [1, 2]. The regeneration of a new growth cone involves many intracellular processes including proteolytic events, cytoskeletal rearrangement, and regulated transport of repair materials [3]. Although progress has been made in identifying causes for abnormal regeneration, additional novel ways to study nerve repair and regeneration following injury can have a significant impact on our understanding of the process.

To investigate the role of growth cones in nerve repair and regeneration a laser microscope system was developed to locally damage axons while simultaneously observing the repair process in real time using phase and fluorescent microscopy. By focusing a short-pulsed picosecond laser beam to a diffraction limited spot, individual axons in cell cultures can be manipulated without damaging adjacent cells. The laser microscope system uses a 532 nm picosceond (ps) laser to partially damage (sub-axotomy) rat hippocampus neurons and human neurons derived from induced pluripotent stems (iPS). Previous preliminary studies on goldfish retinal ganglion cells in culture have shown this approach to be feasible [4, 5]. In the following sections will describe key steps in using a laser ablation approach for neuron repair studies and discuss preliminary results in hippocampus and iPS neurons.

Materials and Methods

Coating coverslips

For sub-axotomy experiments, coverslips were prepared prior to coating. 1oz coverslips were acid washed in a 33%HCL solution and agitated over night. The HCL

solution was washed out using DI water 3 times at 1 hour intervals with agitation. The coverslips were then sterilized by placing coverslips in a 100% ethanol and flamed over a bunsen burner.

Coverslips were placed in a 24 well plate and coated with 250 μL of 0.2 mg/mL Poly-L-Lysine. Dishes were incubated for 3 hours or left to sit overnight at room temperature. Poly-L-Lysine solution was aspirated and washed 3 times using culture grade water at 10 minute intervals. Dishes were dried in a sterile hood before platting cells. The same process was repeated using 35mm gridded imaging dishes (Matek) for immunofluorescences staining.

Primary nerve cell preparation

Primary hippocampal and dorsal root ganglion neurons were dissected from embryonic 17-18 day rats and plated onto coated 35mm imaging cell culture dishes with 0.2 mg/mL poly-l-lysine. Primary neurons were dissected into Hanks Balanced Salt solution (HBSS) containing 10mM HEPES and 1% penicillin/streptomycin and then plated into plating media containing Neurobasal, 2% b27, 1% Glutamax and 5% FBS. The day after dissection, 2/3 of the plating media was replaced with maintenance media containing Neurobasal, 2% b27 and 1% Glutamax. 2/3 of maintenance media was replaced every 2-3 days.

Actin and tubulin fluorescence staining

To visualize real time cytoskeletal repair from laser sub-axotomy, nerve cells were transduced with red fluorescent protein (RFP) tubulin. Nerve cell cultures approximately 3-4 days old were incubated over night with 10 ul of *CellLight* tubulin RFP (C10614, Life Technologies). Cells were also fixed and stained with mouse tubulin and phalloidin. Immediately after laser sub-axotomy, the nerve cells were fixed with 4% PFA for 1 hour at room temperature and washed 3 times using PBS. Next the cells were incubated in a blocking buffer for 30 minutes at room temperature. The tubulin primary antibody was incubated overnight and then washed with PBS 3 times. The secondary antibody against mouse tubulin was incubated for 30 minutes. Phalloiden was diluted to 40:760ul in PBS and incubated in cells for 20 minutes. Cells were washed with PBS and then left in 1mL of PBS for imaging.

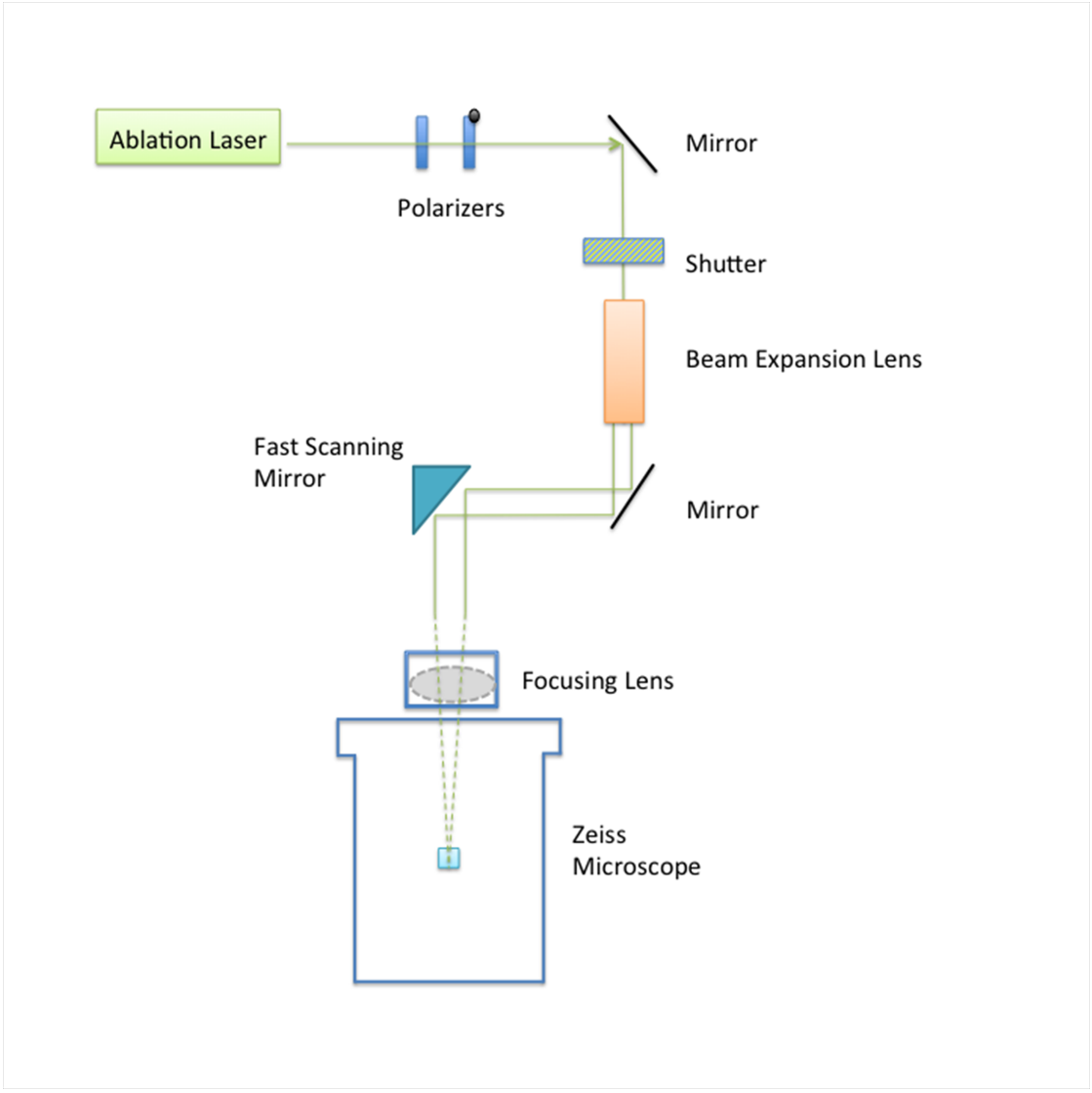

Figure 2.1: Schematic of the optical hardware to direct the laser into the microscope system.

Optical design and hardware: RoboLase

Neuronal repair studies were performed using a robotic laser microscope system (RoboLase) consisting of an ablation laser, external optics to direct the laser path into the microscope, an inverted microscope with a motorized stage, CCD

cameras, and Labview based software to control the optical components as well as phase and fluorescent imaging [6].

The optical set up is described in Figure 2.1. The ablation laser used is a diode-pumped Vanguard Nd: YVO_4 second harmonic generator (SHG) 532 nm laser light linearly polarized with 100:1 purity, 76 MHz repetition rate, 12ps Pulse duration, and 2W average power (Spectra-Physics). A glan linear polarizer (CLPA-12.0-425-575, CVI laser) is positioned after the ablation laser to increase the laser beam polarization purity. The laser beam next passes through a second polarizer mounted in a rotary mount (PR50PP, Newport Corp), which controls the amount of laser power and energy entering the microscope. The motorized mount can rotate the second polarizer to its vertical position for maximum transmission (95%) or to its horizontal position for minimum transmission below the damage threshold of biological samples. The rotary mount is controlled through the motion board in the PXI chassis [8]. A mechanical shutter (Vincent Associates) with a 30ms duty cycle gates the main laser beam resulting in a 30ms burst of pulses that enters the microscope. The number of pulses is calculated based on the pulse rate of the laser [6, 7]. The laser beam passes through an adjustable-beam expander (2-8X, 633/780/803nm correction) and is lowered to a height just above the optical table by using additional mirrors and mirror mounts. A dual-axis fast scanning mirror (FSM-200-01, Newport Corp) is used to steer the laser beam at an imaged plane conjugate to the back focal plane of the microscope objective.

The RoboLase system utilizes a Zeiss axiovert 200M (Zeiss) with the following: motorized objective turret, reflector turret, fluorescent filter cubes,

condenser turret, halogen lamp shuttering with intensity control, mercury arc lamp shutter, camera port selection, objective focus with parfocal switching between objectives. For neuronal ablation experiments a 63X, phase III, Na1.4 Plan-Apochromat oil immersion microscope objective is used. Neurons are mounted on a X-Y stepper stage (Ludl Electronic Products) controlled with a PXI-7344 stepper motion controller (National Instruments) and a MID-7604 power drive. Phase and fluorescent images are acquired through a Hamamatsu Orca_AG deep-cooled 1344×1024 pixel, 12-bit digital CCD camera with digital output (Hamamtsu Photonics). Hammatsu's video Capture library for LabView is used to communicate with the ORCA camera controller through its DCAMPI driver.

The software used to control the microscope, cameras, and external light paths is programmed in the LabVIEW language. The RoboLase software also manages image and measurement file storage. The "Front panel" software of the Robolase system was designed to provide a user friend interface capable of meeting the demands of single cell manipulation (Figure 2.2). A detailed description of the RoboLase Software has been published [8].

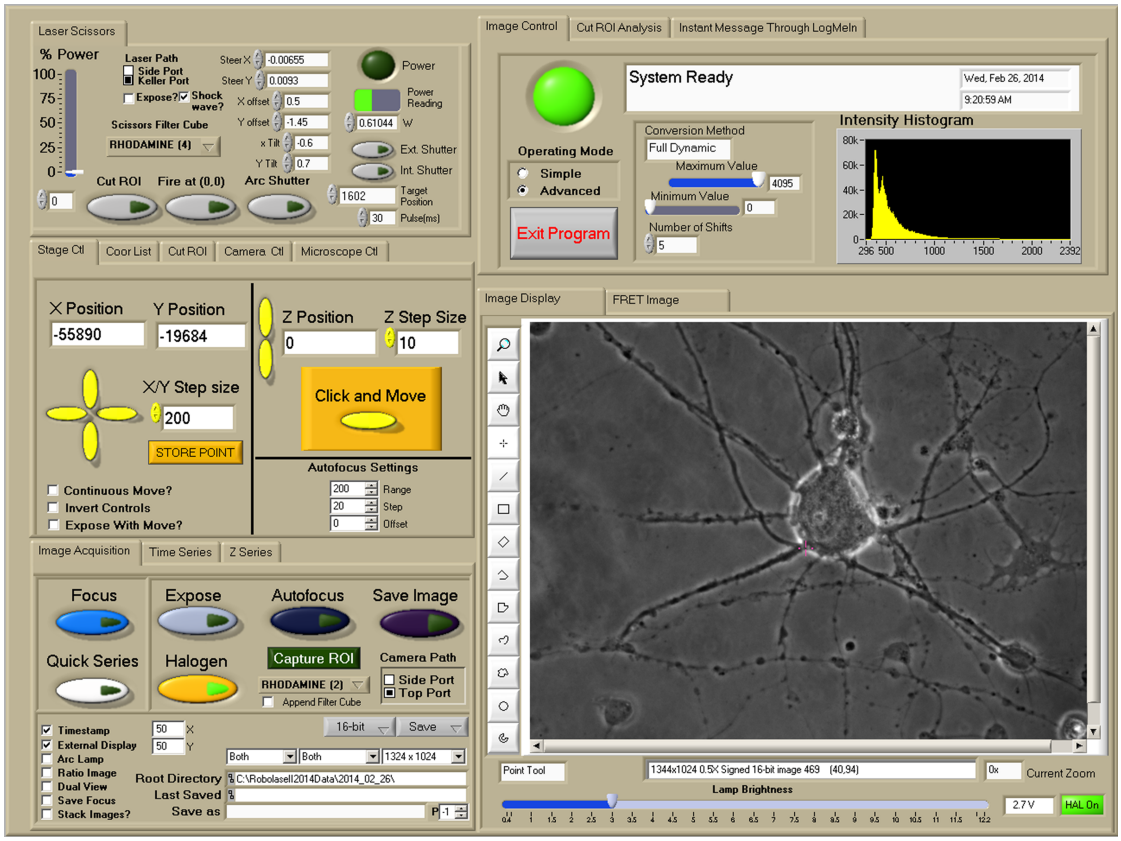

Figure 2.2: Screen shot of the LabView RoboLase interface system to control laser ablation.

Laser power measurement

The laser power was calculate by calibrating the laser power versus polarizer position. Laser power measurements were used for determining the energy and power in the focal spot used to damage axons. To determine the laser power at the focus spot of the objective, the transmittance of the objective is multiplied by the laser power measured at the back aperture. A modified dual objective method is used to calculate the transmission of the objective [9]. This was achieved by first measuring the laser power at the back aperture of the objective (P_{in}) with a photometer (1918-C, Newport or some other suitable power meter). Next, two objectives (A and B) are coaxially

placed such that the lenses are facing each other with emersion oil and a glass coverslip in between the objectives (Figure 2.3). A photometer is used to measure the power exiting the back aperture of objective B (P_{out}). The transmission of the combined objectives is calculated using the following equations:

$$T_1 = \frac{P_{out}}{P_{in}} \quad (1)$$

$$T_1 = T_A \times T_B \quad (2)$$

Where the T_A and T_B equal the transmission of objective A and B respectfully. A third objective is used to determine the transmission of the objectives A and B. Using equations (1) and (2), the following equations can be used to solve the transmittance for 3 objectives (A, B, and C)

$$T_A^2 \times T_B^2 \times T_C^2 = T_1 \times T_2 \times T_3 \quad (3)$$

$$T_A \times T_B \times T_C = \sqrt{T_1 \times T_2 \times T_3} \quad (4)$$

$$T_A = \frac{\sqrt{T_1 \times T_2 \times T_3}}{T_2} \quad (5)$$

$$T_B = \frac{\sqrt{T_1 \times T_2 \times T_3}}{T_3} \quad (6)$$

$$T_C = \frac{\sqrt{T_1 \times T_2 \times T_3}}{T_1} \quad (7)$$

The focus spot power equals (P_{in}) times the transmittance of the objective [10]. Assuming *X* is the power reading that creates the expected laser damage, the energy per pulse is equal to $\frac{X \times Objective\ Transmission}{Laser\ Repetition\ Rate}$. The total laser dosage is energy per pulse × number of pulses per shot × number of spots in the damage.

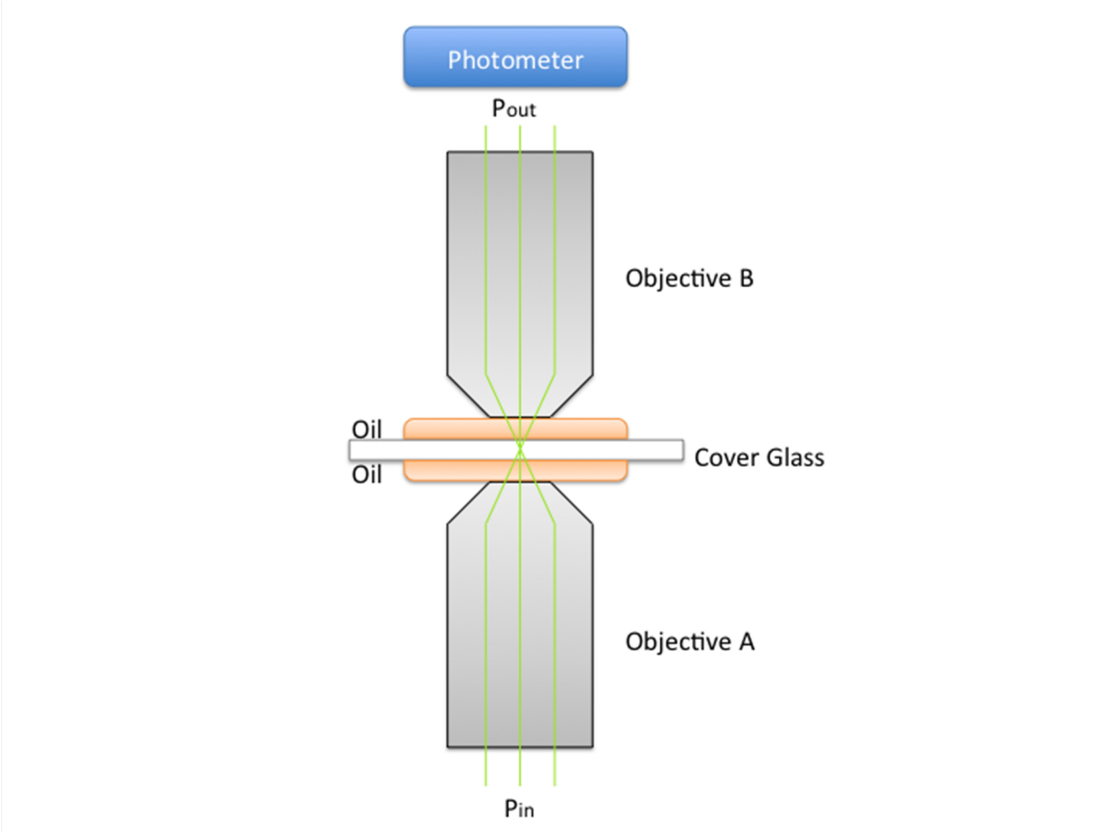

Figure 2.3: Schematic of the dual-objective method.

Results

To perform live imaging of neuronal cells for extended periods of time, the temperature, humidity, and CO_2 concentration of the environment was controlled using a microscope incubator (OkoLab, NA, Italy). The amount of power necessary to create sub-axotomy was determined by targeting a nerve axon at a low laser power and gradually increasing the laser dose until visible thinning of the axon can be seen within a second after laser exposure (Figure 2.4). The power threshold to damage nerve axons for hippocampus and iPS nerve cells was determined to be about 41mW

and 32mW respectfully. Cell cultures used in laser ablation experiments were 3-5 days post dissection. Phase contrast images of the neuron prior to laser ablation to characterize pre-irradiation morphology and behavior. After ablation the axon was followed by using phase contrast of fluorescent imaging immediately after damage for up to 60 minutes.

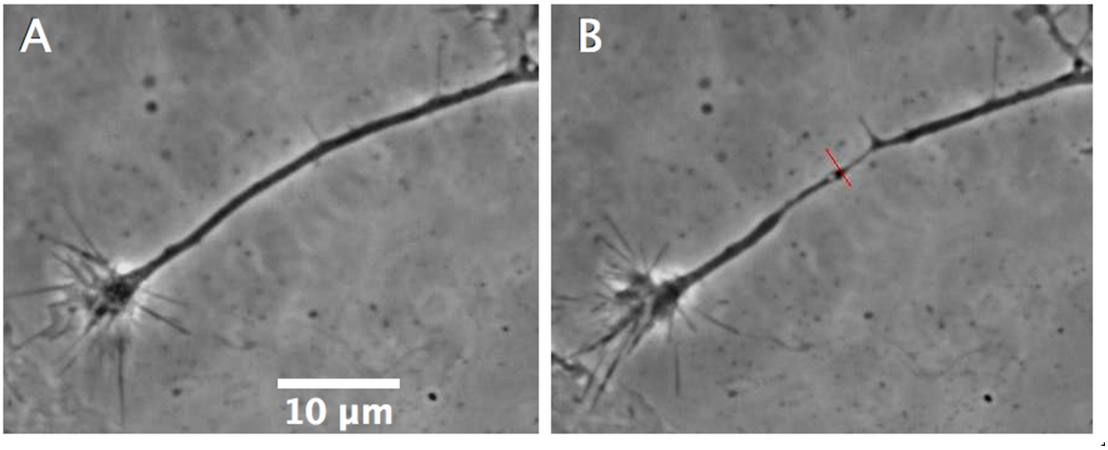

Figure 2.4: Hippocampus thinning after laser damage. Growth cone can be found by looking for structures at the end of nerve axons: lamellipodia can be distinguished by the actin network formed at the leading edge. The slender protrusions that extend outward past the lamellipodia are the filopodia

Phase contrast images from pre and post laser exposure were compiled and analyzed using ImageJ. Phase contrast images of hippocampus and iPS neurons after laser ablation showed a visible thinning of the nerve axon followed by a distinct repair process involving the growth cone and localized cytoskeletal remolding. The growth cone retracted towards the damage site in both hippocampus and iPS nerve cells, possibly providing cytoskeletal material to repair the injured region of the axon. This retraction was more prevalent in iPS neurons where the growth cone would fully retract to the damage site to restore axonal thickness (Figure 2.5).

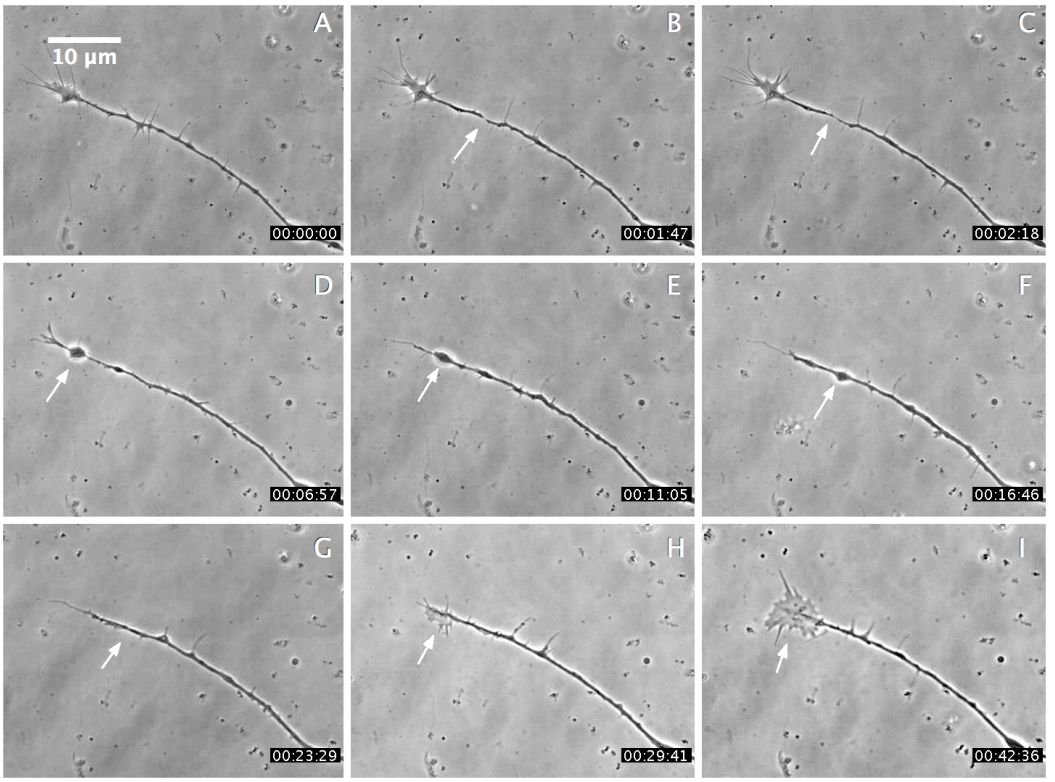

Figure 2.5: iPS nerve cell repair and regeneration. (A) Nerve cell prior to laser ablation. (B) Arrow points to were nerve cell is cut. (B-C) Thinning at the damage (E-G) Axonal thickening and growth cone retraction. (H-I) New growth cone established.

In severely damaged axons in both cell types, the growth cone retracted past the damaged site and did not recover. The observed retraction may be initiated through the release of chemotrophic factors from the damage site, and which initiate axonal repair [4]. In some hippocampus neurons, lamellipodia and filopodia like structures formed at the damage site, or near the cell body traveling towards the damage site probably to assist in the repair of the injured axon (Figure 2.6). This response was exhibited within 5-13 minutes after laser damage. All cells that exhibited this response recovered in axonal thickness and appeared to be healthy.

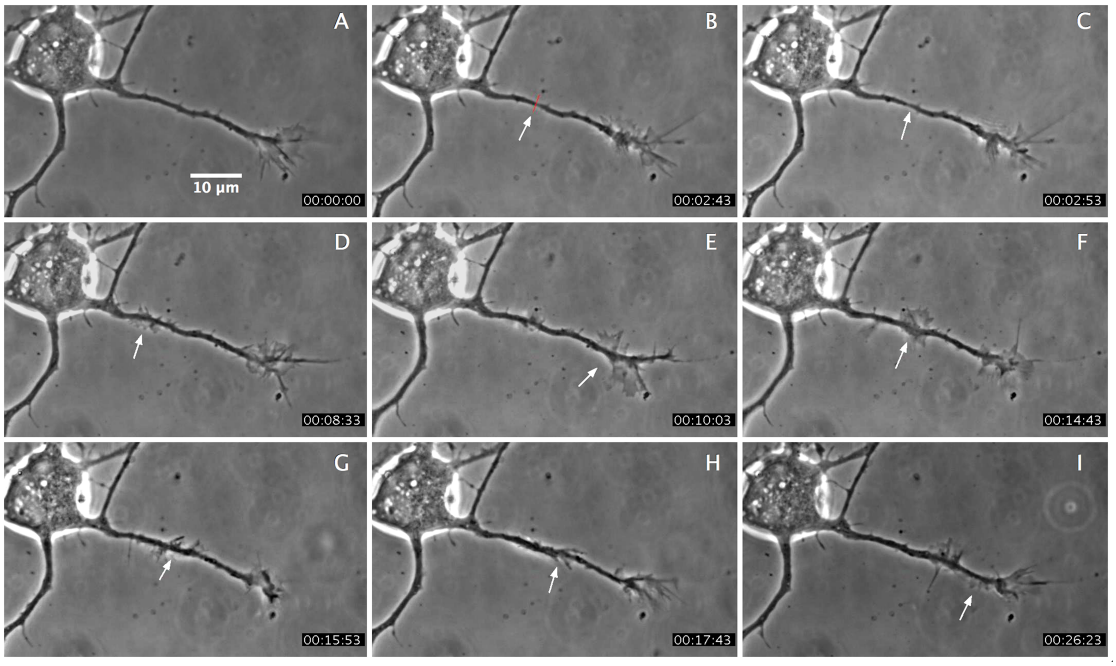

Figure 2.6: Hippocampus nerve cell repair and regeneration. (A) Growth cone before laser sub-axotomy. (B) The axon is damaged along the red line causing a thinning of the axon. (C-D) Axon is slightly thinner at ablation site and actin accumulates at the base of the cell body. (E) Growth Cone retracts slightly and sends repair material towards damage site. (F) The growth cone is reduced in size and actin is accumulated at the damage site. (G-H) Nerve axon thickens and is repaired. (I) Lamellipodia progress forward and combines with the growth cone.

Nerve repair and regeneration was qualitatively scored based on axonal recovery and the growth cone involvement in the repair. For hippocampus neurons a "++" response exhibits extensive axonal cytoskeletal remodeling at damage site and the growth cone aids recovery. A "+"response exhibits axonal repair with some or no involvement of growth cone. A "-" response is when the nerve cell does not recover from laser damage. In hippocampus neurons 41.7% of the cells exhibited a "++" response, 45.8% showed a "+" response, and 12.5% of the neurons did not recover from the laser damage (Table 1). For iPS neurons a "++" score was given to nerve cells that exhibited both axonal repair and growth cone reformation, "+" was given to

nerve cells that exhibited axonal repair with partial or no reformation of growth cone, and "-" was given nerve cells that did not recover from laser damage (Table 2). iPS nerve cells had a "++" response of 21%, a "+" response of 25%, and a "-" response of 54%.

Table 2.1: Hippocampus Neurons (Last 6 Experiments)

Response	Number	Percent
+	11	45.80%
++	10	41.70%
-	3	12.50%
Total	24	100

Table 2.2: iPS Neurons

Response	Number	Percent
+	7	25
++	6	21
-	15	54
Total	28	100

Discussion

The variability in responses and response rates could be related to number of factors such as general health and age of neurons used neurons. Another factor to consider is that the relative thickness of the nerve axon will partially determine the amount of energy absorbed needed to produced significant, but sub-axotomy damage.

The relative damage in proximity to the nerve cell soma has also been shown to effect repair [11]. Both hippocampus and iPS nerve cells were cut approximately 10 um from the nerve cell's growth cone. Although due to the age and length of axonal outgrowth, laser sub-axotomy was closer to cell soma in some neurons than others. The proximity of the laser injury to the cell soma was most notable in hippocampus neurons. In hippocampus neurons where laser damage was closer to the soma, lamellipodia type structures developed near the cell body and propagated down to the damage site (Figure 2.6). This repair process is consistent with results seen by Difato et al using a UVA laser to damage hippocampus neurons [12]. In cells where laser damage was made further away from the cell soma, the growth cone retracted back towards the lesion site and extended filopodia and towards damage site (Figure 2.7). The filopodia seem to fuse with axon to restore axonal thickness, which is very similar to the filopodia response seen previously in goldfish retina ganglion cells. This suggests that there is a wide evolutionary conserved sensing and repair mechanism between species.

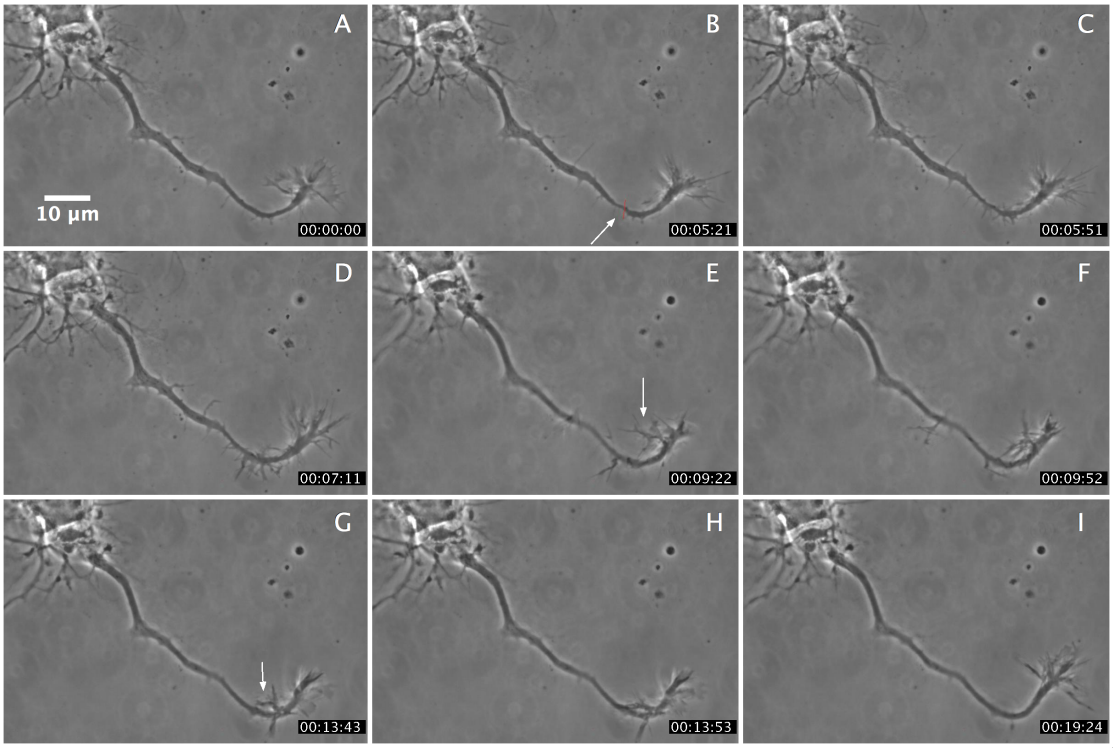

Figure 2.7: Hippocampus growth cone turning. (A) Hippocampus nerve cell before laser ablation. (B) Nerve cell thinned at ablation site. Laser damage directed by the arrow. (C-D) Filopodia like structure forming at damage site. (F-H) Growth cone turning and extending filopodia towards the damage site. (I) Nerve axon repaired

Axonal repair in human iPS nerve cells exhibited a major retraction of the growth cone towards the damage site. After laser sub-axotomy the growth cone retracted into a back to the damage site and fused with the damaged region to restore axonal thickness (Figure 2.5). The repair process for human iPS nerve cells was observed to be about twice as long has hippocampus nerve cells. Human iPS nerve axons were about 3 times the length of hippocampus neurons, which may explain the longer repair times due to the increased distance needed to transport repair materials.

Human iPS nerve cells nerve cells exhibit a lower repair response rate compared to hippocampus cells but are similar to the results seen in goldfish retina ganglion cells. The lower repair response rate could be due to a number of factors. An important consideration is the age of the cell culture. The differentiation process for human iPS cells into the neuronal phenotype is about 4 weeks, which makes the iPS neruons considerably older than the 3-5 day hippocampus cells at the time of laser damage. In addition human cells have been shown to have lower regeneration capabilities to rodent cell types [1]. Lastly it is worth mentioning that human iPS nerve cells are not fully characterized. Whether they can completely mimic normal nerve cells remains to be seen. However the results of the laser sub-axotomy experiments do suggest that the mechanisms for axonal damage repair, do occur in these cells

The laser damage mechanism from laser subaxtomy has not been fully characterized, and may be a combination of single or two photon absorption, or possibly the creation of a plasma and shock wave, all of which likely affect the axon cytoskeletal complex [4]. The axonal thinning produced with the 532 nm ps green laser beam was similar to that observed using a 532 nm ns laser on goldfish retina neurons. Electron micrographs of the retina cells damaged with 532 ns laser showed that the damage did not rupture the cell membrane (Figure 2.8). It appears that the thinning is a result of loss of cytoskeletal structure in the axon even though there was evidence of microtubules in the damage area. However, it is not clear whether or not the microtubules were normal, as they appeared somewhat compressed as viewed in the electron micrographs.

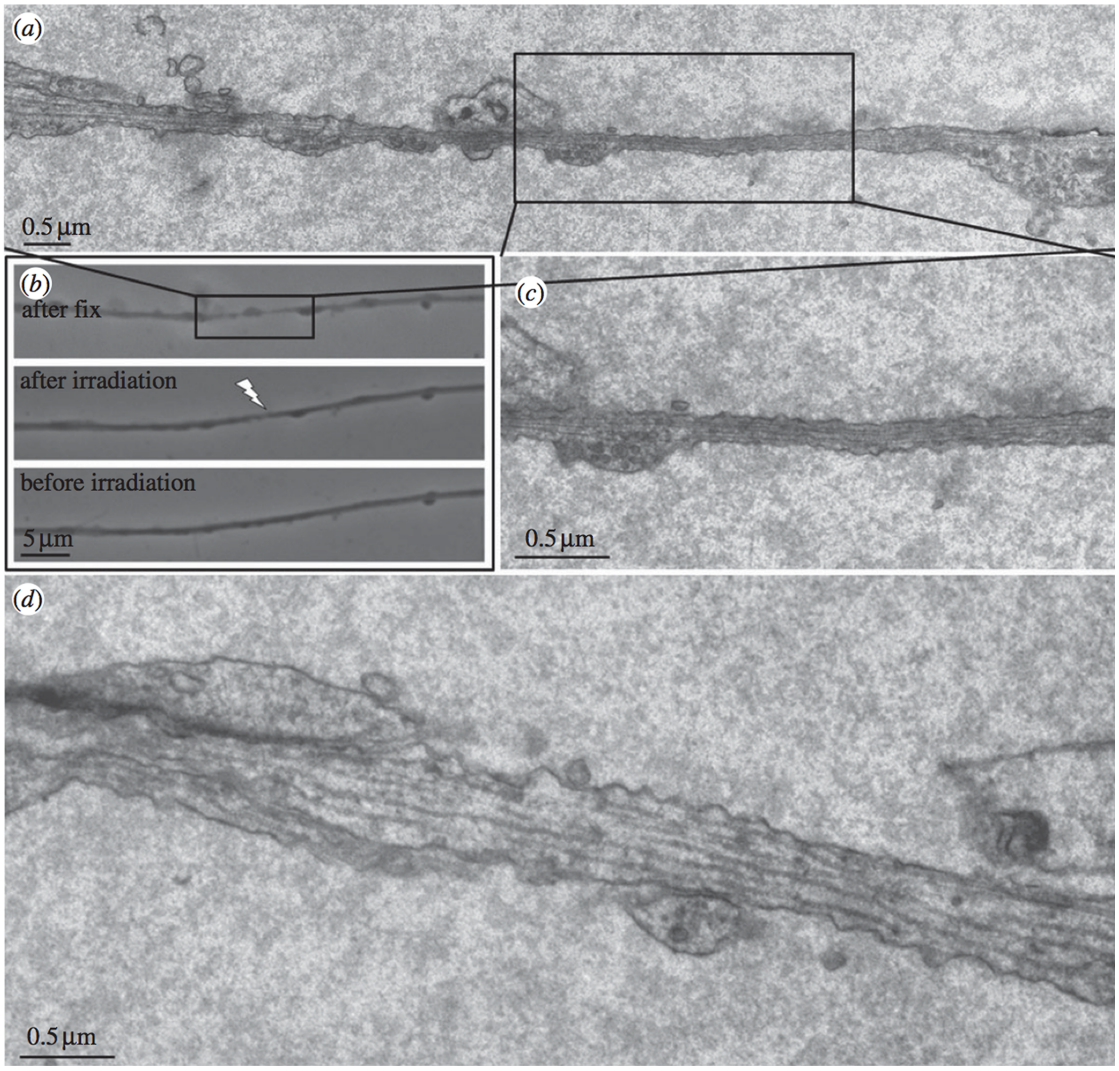

Figure 2.8: TEM and phase contrast images of damaged axon: (A) reconstructed collage of multiple TEM images of an axon fixed 30 s after laser irradiation. (B) Live phase contrast images taken before (bottom) and after irradiation (middle) and after fixation (top). Images are matched with the electron microscope images in (A). (C) Electron micrograph of the region in the center of the 'thinned' zone. Note the intact cell membrane and the presence of contiguous microtubules. (D) Non-irradiated region 36 mm away from the laser-irradiated region (Wu et. al) [4]. Copy Right Royal Society Interface

To further examine the cytoskeletal repair and microtubule damage fluorescently labeled RFP tubulin was monitored before and after laser axotomy. Fluorescent time series analysis showed a visible retraction and accumulation of tubulin at the damage site consistent with the response seen in phase contrast images (Figure 2.9). RFP tubulin signal decreased in intensity at the ablation site, but recovered in intensity as axonal repair proceeded. The fluorescent signal at the damage site indicates microtubule structure was partially preserved after laser sub-axotomy.

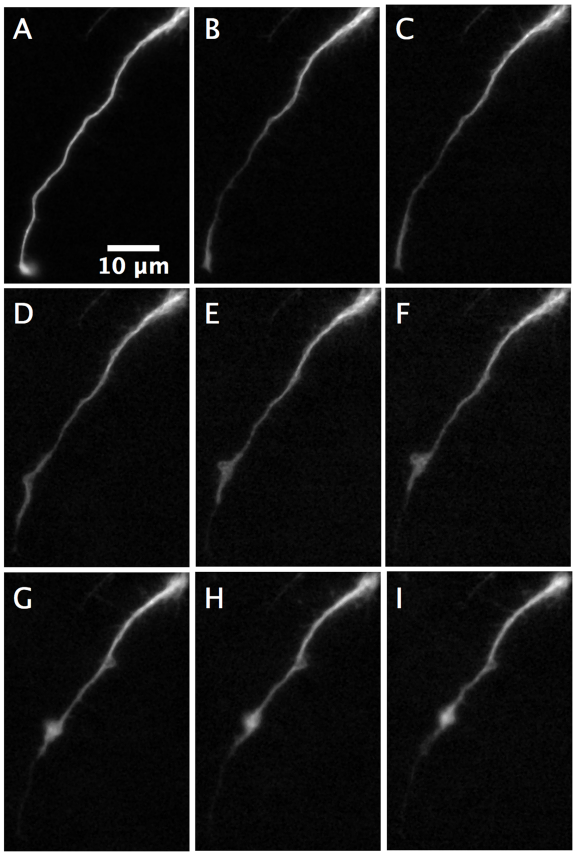

Figure 2.9: Hippocampus neuron transduced with GFP tubulin before and after laser radiation

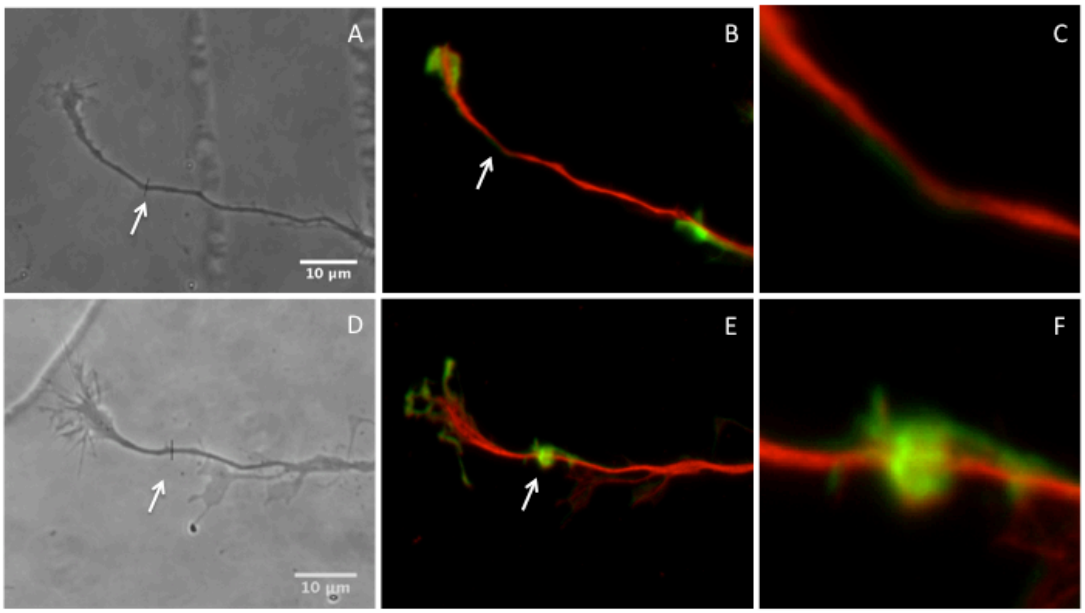

Figure 2.10: Actin and tubulin staining of hippocampus neurons. (A) Phase contrast image of neuron prior to laser ablation. Location of cut is directed by the arrow. (B) Neuron fixed 5 min after cut. The arrow points towards the laser damage. (C) Zoomed picture at the damage site. (D) Phase contrast image of neuron prior to laser ablation. Location of laser cut is directed by the arrow. (E) Neuron fixed 6 min after cut. The arrow points towards the laser damage. (F) Zoomed picture at the damage site.

Hippocampus cells were also fixed at different time points of recovery and stained for tubulin and actin. At the laser ablation site a clear loss of tubulin can be seen in Figure 2.10 consistent with results seen in cells transduced with RFP tubulin. This suggests that laser axotomy damages microtubules and microtubule polymerization is a step in repair of the nerve axon. In cells that were fixed 10 minutes after laser sub-axotomy, a visible actin accumulation at the damage site of the nerve axons can be seen. This is consistent with the repair process seen in phase contrast images and is indicative of the formation of lamellipodia.

Conclusion

In summary, repair responses were observed in rat hippocampus and human iPS nerve cells using controlled laser ablation. These responses were similar to those seen in previous studies on goldfish ganglion cells and suggest that the axon repair mechanism are highly conserved between distant species. Additional studies should be done to elucidate the biochemical pathways involved in growth cone sensing of damage and cytoskeletal remodeling. Experiments using fluorescent calcium dyes or FRET based biosensors could provide insight into the intracellular signaling involved in sensing axonal damage. Several inhibitors such as cytochalasin D, Nocodazole, and ROCK could be used during experiments to help understand the repair pathways. The study of repair pathways at the single cell level can contribute to understanding the repair mechanism necessary to restore damaged neuronal circuits at the tissue and organ levels.

Acknowledgements

This work was supported by funds from the Beckman Laser Institute Inc. Foundation awarded to MWB.

Chapter 2, in part, is a reprint of material as it appears in " Laser Microbeam Targeting of Single Nerve Axons in Cell Culture" Methods in Molecular Biology: Neuronal Cell Death, 2014, Nicholas Hyun, Linda Z. Shi, and Michael W. Berns. The thesis author was the primary investigator and author of this material.

References

1. V.J. Tom, M.P. Steinmetz, J.H. Miller, C.M. Doller, and J. Silver. (2004) Studies on the development and behavior of the dystrophic growth cone, the hallmark of regeneration failure, in an in vitro model of the glial scar and after spinal cord injury. *J Neurosci* **24**, 6531– 6539.

2. A. Erturk, F. Hellal, J. Enes, and F. Bradke. (2007) Disorganized microtubules underlie the formation of retraction bulbs and the failure of axonal regeneration. *J Neurosci* **27**, 9169–9180.

3. F. Bradke, J.W. Fawcett, and E.S. Spira. (2012) Assembly of a new growth cone after axotomy: the precursor to axon regeneration. *Nat Rev Neurosci* **13**, 183-193.

4. T. Wu, S. Mohanty, V. Gomez-Godinez, L.Z. Shi, L.H Liaw, J. Miotke, R.L. Meyer, and M.W. Berns. (2011) Neuronal growth cones respond to laser-induced axonal damage. *J R Soc. Interface*

5. T. Wu, T.A. Nieminen, S. Mohanty, J. Miotke, R.L. Meyer, H. Rubinsztein-Dunlop, and M.W. Berns. (2012) A photon-driven micromotor can direct nerve fibre growth. *Nat Photonics* **6**, 62-67.

6. E.L. Botvinick, and M.W. Berns. (2005). Internet-based robotic laser scissors and tweezers microscopy. *Microsc Res Tech* **68**, 65-74.

7. M.W. Berns, E.L. Botvinick, L. Liaw, C. Sun, and J. Shah. (2005). Micromanipulation of chromosomes and the mitotic spindle using laser microsurgery (laser scissors) and laser-induced optical forces (laser tweezers). In: *Cell biology: a laboratory handbook*. Burlington, MA. Elsevier Press.

8. L. Shi, M.W. Berns, and E.L. Botvinick. (2008) RoboLase: Internet-accessible robotic laser scissor and laser tweezers microscope system" Medical Robotics, I-Tech Education and Publishing, ISBN 978-3-902613-18-9.

9. H. Misawa, M. Koshioka, K. Sasaki. N. Kitamura, and H. Masuhara. (1991) Three-dimensional optical trapping and laser ablation of a single polymer latex particle in water. *J Appl Phys* **70**, 3829-3836.

10. V. Gomez-Godinez, T. Wu, and A.J. Sherman. (2010) Analysis of DNA double-strand break response and chromatin structure in mitosis using laser microrradiation. *Nucl Acid Res* **38**, e202.

11. K.J. Fernandes, D.P. Fan, B. J. Tsui, S. L. Cassar, and W. Tetzlaff. Influence of the axotomy to cell body distance in rat rubrospinal and spinal motorneurons: differential regulation of GAP-43, tubulins, and neurofilament-M. *J. Comp Neurol*. 414, 495–510 (1999).

12. F. Difato, H. Tsushima, M. Pesce, F. Benfenati, A. Blau, and E. Chieregatti. (2011) The formation of actin waves during regeneration after axonal lesion is enhanced by BDNF. *Scientific Repor*t